Performance of Graphite/SiO₂ Composites as Cathode Electronic Active Layer in Al-Air Batteries

H. Aripin
Department of Electrical Engineering,
Faculty of Engineering,
Siliwangi University
Tasikmalaya, Indonesia
aripin@unsil.ac.id

Nurul Hiron
Department of Electrical Engineering,
Faculty of Engineering,
Siliwangi University
Tasikmalaya, Indonesia
hiron@unsil.ac.id

Nundang Busaeri
Department of Electrical Engineering,
Faculty of Engineering,
Siliwangi University
Tasikmalaya, Indonesia
nundangb@unsil.ac.id

Firmansyah M S Nursuwars
Department of Informatics,
Faculty of Engineering,
Siliwangi University
Tasikmalaya, Indonesia
firmansyah@unsil.ac.id

Linda Faridah
Department of Electrical Engineering,
Faculty of Engineering,
Siliwangi University
Tasikmalaya, Indonesia
lindafaridah@unsil.ac.id

Svilen Sabchevski
Lab. Plasma Physics and Engineering,
Institute of Electronics of the Bulgarian
Academy of Sciences
Sofia, Bulgaria
sabch@ie.bas.bg

Abstract— **In this study, the graphite/SiO2 composite performance used as an active electronic layer in an air cathode of an aluminum-air battery (Al-air battery) has been investigated. The effects of the guar gum (GG) binder content of the samples on their characteristic impedance and discharge capacity of an Al-air battery have been analyzed in the interval from 10 to 40%. The characterization of their experimental data was obtained using Electrochemical Impedance Spectroscopy (EIS), Cyclic Voltammetric (CV), and Battery Testing System (BTS). It has been found that the characteristic impedance increases with increasing of the binder content. The sample with the lowest GG content provides the larger discharge capacity of the battery up to 42.54 mAh/g. This observation has been collaborated by an analysis of the CV curve, and it provides an explanation for the increase in the integrated area of the voltammetric curve by a decreased content of the GG binder. As a whole, the experimental results demonstrate that the graphite/SiO₂ composite is an appropriate electronic active material for air cathodes in Al-air batteries. The obtained data can be used for an envisaged further optimization of the properties of this promising material.**

Keywords—graphite/SiO₂ composites, electronic active layer, characteristic impedance, discharge capacity, air cathode, Al-air battery

I. INTRODUCTION

The inability of renewable energy sources to produce energy continuously is one of the serious technical problems in renewable energy power plants, especially from wind and the sun. It is known that the sun does not shine during the night and cloudy weather. The gusts of wind are often fluctuating and have no stable speed, and when the latter is low, it is unable to turn the turbines. Therefore, in such cases, the sun and the wind do not produce energy. To overcome this problem, electrical energy storage devices are needed. Batteries are portable and compact devices for storing electrical energy over a long period. They use chemical compounds capable of generating a charge. Among all known batteries, metal-air batteries are considered promising storage devices that can provide a high specific energy capacity.

Additionally, they are economically viable because a wide variety of cheap materials can be used for their anodes and their cathodes use oxygen from the ambient air together with suitable (usually aqueous) electrolyte. One of the most attractive varieties of the metal-air cells is the Al-air battery

due to its high theoretical specific capacity of 2.98 Ah/g, high voltage (2.7 V), and energy density (8.1 kWh/kg) [1]. Moreover, aluminum anode usage is advantageous since aluminum is inexpensive, abundant, environmentally friendly material, which can be recycled easily. During the electrochemical reactions, however, the metal electrode is oxidized, and the resulting oxide precipitates on the surface of the cell, which leads to a degradation of its performance (e.g., lower capacity). One effective way to suppress the oxide's accumulation on the cathode is to coat it with an appropriate active material. Such material must also provide a channel for the reaction between the water in the electrolyte and the oxygen so that OH⁻ ions are produced on the cathode surface. This requires a porous conducting material with a pore structure that affects the discharge capacity, energy density, and life cycle of the battery favorably.

The carbon-based materials are considered the most promising material to replace Pt-based electrocatalyst due to their availability, excellent electric conductivity, and easy preparation. Many studies have been carried out to investigate the electrochemical characteristics of the carbon and its applicability as an active electrode layer. For example, the cathode's carbon electrocatalyst indicates a significant gain in generating a high discharge capacity with a long stable plateau voltage [2]-[4]. Recently, MnO_2 and activated carbon composite were used to prepare a catalyst of an air cathode [5], [6]. MnO is characterized by high oxygen mobility and high electrical conductivity and exhibits a sufficient electrocatalytic activity for an oxygen reduction. In another study, carbon-coated graphite was used as a negative electrode of various alkaline batteries providing a fast charge transfer at the interface of the graphite and the electrolyte [7] and a high reversible discharge capacity [8]. In these batteries, binders are used to make an active layer that forms a single mechanical unit with sufficient stability of the current collector plate. However, in the presence of a binder, the carbon particles form agglomerates during the active layer's slurry preparation. This causes an uneven pore distribution, caking, bridging, lumping within the agglomerates, thus produce the mesopores with high specific surface area and narrow pore size distribution. As a result, they limit O_2 diffusion and electrolyte access to the active site surface at the air cathode.

SiO$_2$ is a feasible candidate as an active material for oxygen reduction in electrochemical storage devices. This material has been successfully employed in the lithium-ion battery [9], [10], fuel cell [11], Zn air battery [12], and a lithium-air battery [13]. It has been found that the theoretical capacity for silicon and silicon oxides are 4200 mAh/g and 1965 mAh/g, which exceeds by several times the capacity of such conventional anode as graphite. However, the detailed analysis of the experimental data reveals the role of its electric insulating properties and shows that silica with characteristic conductivity of about $10^{-4}\,\mathrm{S\,m^{-1}}$ prohibits a high charge-transfer [14]. Similar adverse effects can also be caused by the volume change of more than 300% during the electrochemical reaction, which leads to particle pulverization, loss of electrical contact with the conductive additive or the current collector, and even peeling off from the current collector [15], [16]. In order to overcome these adverse effects, additives that improve the poor electrical conductivity and suppress an extreme volume change were used. In this study, graphite and SiO$_2$ composites were employed as an active layer of the air electrode in an Al-air battery. The used amorphous SiO$_2$ is characterized by both micro and mesopores [17], [18]. Such material with an appropriate porosity (pore sizes) provides channels for oxygen reduction and electrolyte diffusion. In this paper, we report the research results focused on the preparation of an active electronic layer based on SiO$_2$, the investigation of the loading of GG binder on the graphite/SiO$_2$ composite, and their influence on the characteristic impedance and discharge capacity of the Al-air battery.

II. EXPERIMENTAL PROCEDURE

A. Preparing the active layer

The active layer's raw materials are commercially available graphite and SiO$_2$ powder, which were supplied from Sigma Aldrich with -325 mesh in particle size. For preparing the active layer, 90% of the graphite and SiO$_2$ composite powder were mixed with 10% GG. The graphite composition in the composites was set as high as 10% for each sample. GG powder was used as a binder. It was dissolved in deionized water and stirred to ensure a good homogenization of the binder suspension. The composite powder has been added slowly into the solution containing GG and stirred to make an appropriate viscous slurry and then ultra-sonicated to break down the agglomerates. The obtained slurry was coated on the nickel mesh and dried at 105°C for 24 hours, and then after drying, it was stored in a desiccator for further treatment. We will refer to the sample prepared in such a manner as GG-10%, while the others (prepared at concentrations 20%, 30%, 40% of GG) as GG-20%, GG-30%, and GG-40%, respectively.

B. Method for assembling and characterizing the Al-air battery

Fig. 1 shows a schematic drawing of the Al-air battery structure used in our electrochemical experiments. The battery cell comprises two rectangular electrodes, namely an anode and a cathode with sizes of 5 x 6 cm^2, and a porous separator membrane (made of tissue truwipes) inserted between them. An aluminum sheet (alloy 1100) was selected as anode material and the active layer attached to a nickel 300 mesh substrate as an air cathode. The used electrolyte is an aqueous solution of 1 M KOH, which was injected into the separator. The battery was clamped between Acrylic sheets,

not shown in the figure. Two terminals from the aluminum sheet and nickel meshes that serve as current collectors were used to measure the EIS, CV, and cell discharge. The prepared cells' EIS and CV measurements were performed using a potentiostat/ galvanostat/impedance analyzer (PalmSens4). EIS was carried out using a small amplitude AC signal of 10 mV at a range of frequencies from 105 to 10^{-2} Hz to investigate the electrode interface in the cell after each charge and discharge cycle. The impedance data were analyzed by using Nyquist plots. The polarization resistance was extracted from the diameter of the semicircle in the Nyquist diagrams. The impedance plots were fitted using PalmSens Trace-corrosion mode software. The CV with a scan rate of 0.05 V/s from 0 to 2.5 V was performed at room temperature. In the forward scan, referred to as an anodic trace, the potential was swept from 0 to 2.5 V. Then, the scan direction was reserved, and the potential was swept back to 0 V, referred to as the cathodic trace. The constant current discharging tests were performed using a multichannel battery testing system (BTS-MPTS, China) at a discharge current of 0.5 mA. The cells were discharged to a cutoff voltage of 0.05 V at room temperature.
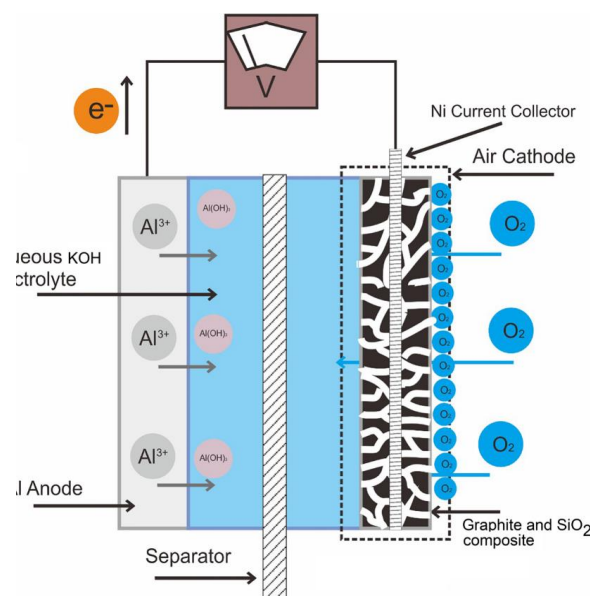

Fig. 1. A schematic drawing of the Al-air battery structure

III. RESULTS AND DISCUSSION

Fig. 2 shows Nyquist plot of EIS and the equivalent circuit model of the fitted data for Al- air batteries using an active layer at different GG contents in 1 M KOH electrolyte. The R_s and W are associated with the electrolyte solution and Warburg diffusion resistances while R_{ct} and CPE$_{dl}$ are the charge transfer resistance and double layer capacitance of the cathode/electrolyte interface, respectively. Fig. 2a shows that GG-10% exhibits a very small semicircle in the high frequency region, that is correlated to a very low R_{ct}. As the frequency decreases, the entire Nyquist plot becomes a straight line, which is attributed to W in the active layer [19]. It appears as an incomplete semicircle in the high frequency region. The active layer containing GG from 30% to 40% had a relatively larger diameter of the semicircle than that of the active layer containing 10% GG. This indicates that the active

layer's surface is partially or totally blocked to the electron transfer by the charge carrier. The highest fractions of 40% lead to an even stronger blockage of the layer surface. Furthermore, the GG content increase affects both the length and slope of the straight line observed in the low-frequency range. The straight line's length in the impedance spectrum of the active layer increases with the increase of GG content. Such observation is related to an increase in the W that is an intrinsic resistance of the active layer. The line slope of GG-10% is greater than the one of GG-20%. This suggests that GG-10% has a more rapid diffusion of electrolyte ions in the active layer. It can also be observed that the line slope is almost the same for GG-20%, GG-30%, and GG-40%, which indicates the same rate of diffusion of the electrolyte ions entering the pore channels of the active layer. Table 2 shows the obtained parameters from the fitting of EIS data for Al-air batteries. The values of R_s, R_{ct}, and W for GG-10% are much smaller compared with those corresponding to a higher (>10%) content of GG. This means that GG-10% possesses a more stable surface and a faster charge transfer process that leads to an enhanced discharge capacity. The notable increase in R_{ct} for a GG content of more than 20% indicates that the formed active layers are characterized by a higher kinetic barrier for the electrolyte ions insertion, resulting in poor electrochemical performance.
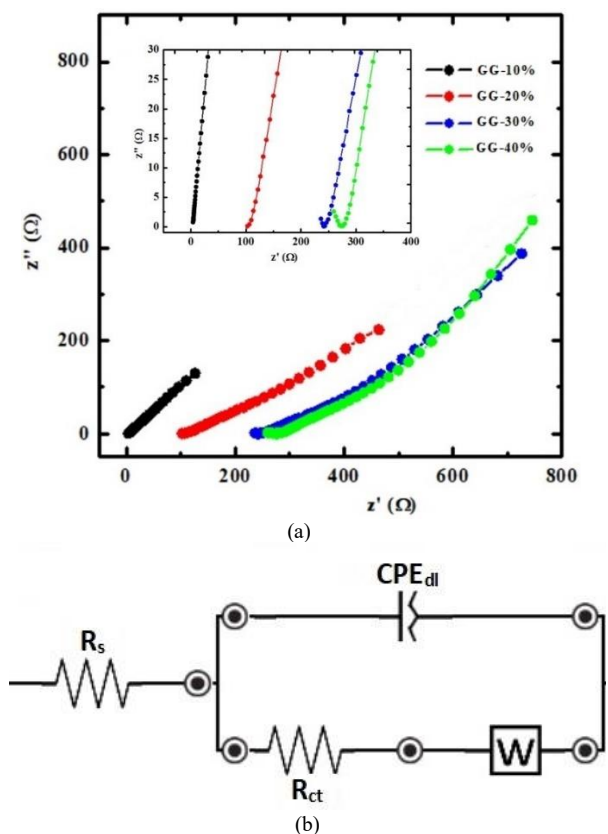
evolution reaction (OER) process, a minute peak is observed at about 1.76 V for GG-10%, and when the content increases up to GG-40%, the peak shifts to a lower potential. The minute peak's presence indicates that the KOH electrolyte solution has a low activity concerning O_2. During the oxygen reduction reaction (ORR) process from 2.5 and 0 V, a broad peak for all sample is also observed at the same relative position of about 1.6 to 1.8 V. It is attributed to the emptying of OH^- ions from the pores and the formation of aluminum hydroxide as the charge carrier [20]. It can be seen that large cathodic and anodice currents are observed for GG-10%, and they are reduced when the content exceeds GG-10%. For content ranging from GG-20% to GG-40%, the cathodic currents become comparable (about –1.5 mA), whereas anodic current decreases as GG's content increases. The observed current's significant increase is attributed to an increased volume of the mesopores in the active layer. The high mesoporosity allows for an increase in the number of ordering transitions within the bulk of the electrolyte and speeds up the active layer's electrolyte degradation. This assumption is supported by some published data, which demonstrates that the peak currents depend strongly on the mesoporous volume for Aerosil®-templated carbon material with varying sucrose content [21]. Henceforth, it was also found that the integrated area of the respective voltammetric curve decreases with increasing the content of GG. These areas are attributed to the available charge and discharge capacity during the scan. An increase of both the cathodic and anodic currents arises from the O_2 reduction.

| Sample type	R_s (Ω)	R_{ct} (Ω)	W (Ω)	CPE_{dl} ($\mu F\ s^{n-1}$)
GG-10%	4.13	0.02	86.21	19.61
GG-20%	102.89	3.82	210.34	11.87
GG-30%	236.45	18.41	278.52	4.55
GG-40%	259.39	53.25	332.41	1.14

Fig. 2. (a) Nyquist plot of EIS and (b) the equivalent circuit model of the fitted data for Al-air batteries using active layers with different GG contents in 1 M KOH electrolyte.
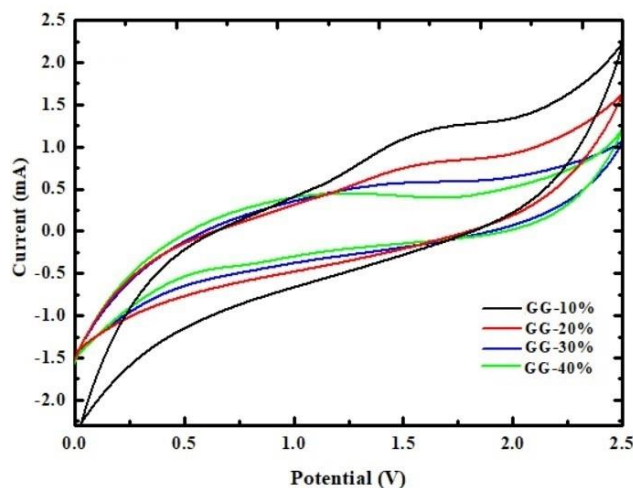

Fig. 3. CV curves for Al-air batteries using active layers with different GG contents in 1 M KOH electrolyte.

Fig. 3 shows CV curves for Al-air batteries using active layers with different GG contents in 1 M KOH electrolyte. The measurements of CV were recorded in the range of voltage window from 0 and 2.5 V at a scan rate of 1 mV/s. The CV curve shows a similar capacitive shape. During the oxygen

Fig. 4a shows a discharge curve for Al-air batteries using active layers with different GG contents in 1 M KOH electrolyte. The cell voltage increases in the initial stage of the discharge curve. This phenomenon can be explained by the formation of the charge carrier layer during the charging process's initial reaction, which forms a barrier to the flow of

138

ions through the electrode, hence reducing the access to the active material. With the increase of GG contents, a progressive decline in the discharge voltage was observed. It was related to the measured R_s resulting from depletion of the KOH electrolyte solution due to absorption by the GG binder. The high discharging voltage is related to the shift in ORR's onset potential in the CV results, as shown in Fig. 2. It is important to note that the voltage profile exhibits a plateau at 1.08 V, 0.95 V, and 0.8 V for GG-10%, GG-20%, GG-40%, respectively, and a sloped region between 0.9 V and 0.78 V for GG-30%. The most notable difference can be seen in the plateau's length, which significantly decreases with the increase of GG content. This difference probably corresponds to an increase in the active layer's internal resistance due to electrolyte decomposition and charge carrier products plugging the pore channel, thereby blocking access to the inner silicon active sites. These results are similar to the results observed for lithium batteries [22], Fe-air battery [23], and Al-air battery [24]. In Fig. 4b, for GG-10%, the specific discharge capacity is 42.54 mAh/g. As GG's content from 20% to 40%, the capacity decreases from 38.81 to 18.06 mAh/g. The measured Rct and W may explain such a decrease in the Al-air battery.

It can be seen from Tabel I and Fig. 3, that when the GG content increases, the values of R_{ct} and W also increase, which tends to decrease the discharge capacity as well. The contribution of R_{ct} to the reduction in capacity is smaller than that of W. Due to the fact that the hydroxyl ions diffusion at the open pores is stronger than in the interior during charge and discharge reactions, this results in lower R_{ct} values. Furthermore, we assumed that in most of the interior pores, the hydroxyl ions' diffusion process is dominated by small mesopores and micropores. These pores are only essential for allowing the oxygen ions and a smaller amount of the electrolyte ions to diffuse toward the reaction sites. Only oxygen dissolved in the electrolyte participates in the charge transfer process. This is due to the full or empty state of micropore and smaller mesopore volumes, thus making it more difficult for hydroxyl ions to embed or detach from the pores channel and result in an increased diffusion resistance. This implies that W is more influential than R_{ct} on the discharge performance of the Al-air battery. Such a conclusion is also supported by the corresponding current-voltage curves, as shown in Fig.3, where the limiting current for ORR activity decreases from 25 mA to 0.5 mA. A decrease in the current indicates a decrease in the diffusion rate.

IV. CONCLUSIONS

Presented experimental results indicate that the graphite/SiO$_2$ composite is a promising material for the active electronic layer of the air cathodes used in the Al-air batteries. Such a conclusion is based on the obtained structural and electrochemical properties of the studied samples.

The results of the electrochemical experiments demonstrate a clear correlation between the variation in the characteristic impedance of an equivalent circuit (inflicted by changing the GG binder content) and the corresponding changes in the discharge capacity of the Al-air cells. In particular, it has been found that the sample with the lowest binder content provides the highest discharge capacity of 42.54 mAh/g. Furthermore, the measured discharge capacity decreases from 42.54 to 18.06 mAh/g as the binder content rises to GG-40%. These discharge capacity changes are attributed to the corresponding variations of the R_s, R_{ct}, W, and

CPE_{dl}. It has been confirmed by the CV curve that the integrated area of the voltammetric curve in the samples loaded with a larger content of GG binder is smaller than the areas of the samples loaded with a smaller content of the GG binder.

We envisage a continuation of this study in order to get a deeper insight into the underlying processes and factors that determine the quality (as well as the possibilities for its optimization) of graphite and SiO$_2$ used as an active electronic layer of air-cathodes in Al-air batteries.

REFERENCES

[1] Y. Liu, Q. Sun, W. Li, K. Adair, J. Li, and X. Sun, "A comprehensive review on recent progress in aluminum–air batteries," Green Energy & Environment, vol. 2, pp. 246-277, July 2017.

[2] S. Liu, S. Liu, and J. Luo, "Carbon-based cathodes for sodium-air batteries, New Carbon Mater.," vol. 31, pp. 264 – 270, June 2016.

[3] P. Kaur, G. Verma, and S. Sekhon, "Biomass derived hierarchical porous carbon materials as oxygen reduction reaction electrocatalysts in fuel cells," Prog. Mater. Sci., vol. 102, pp. 1–71, May 2019.

[4] J. Tang, Y. Wang, W. Zhao, R. Zeng, T. Liu and S. Zhou, "Biomass-derived hierarchical honeycomb-like porous carbon tube catalyst for the metal-free oxygen reduction reaction," J. Electroanal. Chem., vol. 847, pp. 113230, Agustus 2019.

[5] R. Koc and S. Ozkececi, "The fabrication of exfoliated graphite sheet-based air cathodes and gel electrolyte for metal-air batteries," Energy Sources, Part A: Recovery Util. Environ. Eff., vol. 41, pp. 1 – 11, November 2018.

[6] S. Wei, H. Liu, R. Wei, and L. Chen, "Cathodes with MnO2 catalysts for metal fuel battery," Front. Energy, vol. 13, pp, 9 – 15, February 2019.

[7] V. Sharova, A. Moretti, G. Giffin, D. Carvalho and S. Passerini, "Evaluation of Carbon-Coated Graphite as a Negative Electrode Material for Li-Ion Batteries," J. Carbon Research, vol. 3, pp. 22, July 2017.

[8] C. Jo, S. An, Y. Kim, J. Shim, S. Yoon and J. Lee, "Nano-graphite functionalized mesocellular carbon foam with enhanced intra-penetrating electrical percolation networks for high performance electrochemical energy storage electrode materials," Phys. Chem. Chem. Phys., vol. 14, pp. 5695–5704, March 2012.

[9] Y. Zhao, Z. Lui, Y. Zung, A. Mentbayeva, X. Wang, M. Maximov, B. Lui, Z. Bakenov, and F. Yin, "Facile Synthesis of SiO$_2$@C Nanoparticles Anchored on MWNT as High-Performance Anode Materials for Li-ion Batteries," Nanoscale Res. Lett., vol. 12, pp. 459 - 466, December 2017.

[10] X. Su, Q. Wu, J. Li, X. Xiao, A. Lott, and W. Lu, "Silicon-Based Nanomaterials for Lithium-Ion Batteries: A Review," Adv. Energ. Mater., vol. 4, pp. 1 - 23, January 2014.

[11] H. Asghar, M. Iqbal, and M. Iqbal, "Silicon-based carbonaceous electrocatalysts for oxygen reduction and evolution properties in alkaline conditions," SN Appl. Sci., vol. 1, pp. 1396 - 1406, October 2019.

[12] X. Cai, L. Lai, J. Lin, and Z. Shen, "Recent Advances in Air Electrode for Zn-air Batteries: Electrocatalysis and Structural Design, Mater. Horizons," vol. 4, pp. 945 -976, July 2017.

[13] V. Roev, S. Ma, D. Lee, and D. Im, "Lyophobized Ordered Mesoporous Silica Additives for Li-O2 Battery Cathode, J. Electrochem. Sci. Technol.," vol. 5, pp. 58 – 64, Juny 2014.

[14] M.N. Obrovac and V.L. Chevrier, "Alloy negative electrodes for Li-ion batteries," Chem. Rev., vol. 114, pp. 11444 - 11502, November 2014.

[15] M. Ko, S. Chae, J. Cho, "Challenges in accommodating volume change of Si anodes for Li-ion batteries." Chem. Electro. Chem., vol. 2, pp. 1645–1651, August 2015.

[16] M. Ashuri, Q. Hea and L. Shaw, "Silicon as a potential anode material for Li-ion batteries: where size, geometry and structure matter," Nanoscale, vol. 8, pp. 74–103, November 2015.

[17] H. Aripin, S. Mitsudo, I.N. Sudiana, S. Tani, K. Sako, Y. Fujii, T. Saito, T. Idehara, S. Sabchevski, "Rapid Sintering of Silica Xerogel Ceramic derived from Sago Waste Ash Using Submillimeter Wave Heating of a 300 GHz CW Gyrotron, J. Infrared Millim. Terahertz Waves," vol. 32, pp. 867 – 876, June 2011.

[18] H. Aripin, S. Mitsudo, E.S. Prima, I.N. Sudiana, S. Tani, K. Sako, Y. Fujii, T. Saito, T. Idehara, S. Sano, B. Sunendar, S. Sabchevski, "Structural and Microwave Properties of Silica Xerogel Glass-Ceramic Sintered by Sub-millimeter Wave Heating using a Gyrotron, J. Infrared Millim. Terahertz Waves," vol. 33, pp. 1149 – 1162, July 2012.

[19] G. Barbero and I. Lelidis, "Analysis of Warburg's impedance and of its equivalent electric circuits," Phys. Chem. Chem. Phys., vol. 19, pp. 24934-24944, August 2017.

[20] P.S.D Brito and C.A.C.Sequeira, "Cathodic oxygen reduction on noble metal and carbon electrodes," J. Power Sources, vol. 52, pp. 1 – 16, November 1994.

[21] K. Schutjajew, R. Yan, M. M. Antonietti, C. Roth, M. Oschartz, "Effects of Carbon Pore Size on the Contribution of Ionic Liquid Electrolyte Phase Transitions to Energy Storage in Supercapacitors," Front. Mater., vol. 6, pp. 1 - 12, April 2019.

[22] M. Baloch, P. Kubiak, V. Roddatis, O. Bondarchuk, C. Lopez, "Processing nanoparticle–nanocarbon composites as binder-free electrodes for lithium-based batteries," Mater. Renew. Sustain. Energy, vol. 21, pp. 1 – 8, November 2017.

[23] K.Vijayamohanan, A.K.Shukla, S. Sathyanarayana, "Kinetics of electrode reactions occurring on porous iron electrodes in alkaline media," J. Electroanal. Chem. Interf. Electrochem., vol. 295, pp. 59 - 70, November 1990.

[24] R. Mori, "A novel aluminium–air secondary battery with long-term stability," RSC Adv., vol. 4, pp. 1982 – 1987, January 2014.